Supplementary Materials

Appendix S1

The adsorption rate R (%) and the amount of adsorbed metal ions (Cr(VI) or Sb(V)) on per gram of adsorbent (Q_t (mg/g)) in time t was calculated by the following equations, respectively:

$$R(\%) = \frac{C_0 - C_t}{C_0} \times 100 \quad , \qquad \text{(S1)}$$

$$Q_t\left(mg/g\right) = \frac{C_0 - C_t}{m} \times V \quad , \qquad \text{(S2)}$$

where C_0 is the initial concentration (mg/L), and C_t is the concentration in time t; V is the solution volume (L) and m is the mass of the used adsorbent (g).

The desorption capacity (Q_{de}, mg/g) and efficiency (R_{de}, %) was calculated by the following equations, respectively:

$$R_{ad.r} = \frac{C_0 - C_{ad}}{C_0} \times 100\% \quad , \qquad \text{(S3)}$$

$$R_{de.r} = \frac{Q_{de.r}}{Q_{ad.r}} \times 100\% \quad , \qquad \text{(S4)}$$

$$Q_{ad.r} = \frac{\left(C_0 - C_{ad}\right) \times V_{ad}}{m} \quad , \qquad \text{(S5)}$$

$$Q_{de.r} = \frac{C_{de} \times V_{de}}{m} \quad , \qquad \text{(S6)}$$

where: r-cycle times, *ad.*-adsorption, *de.*-desorption, V-volume (L), C-concentration (mg/L), Q-adsorption (desorption) capacity (mg/g), m-mass of the adsorbent (g), R-adsorption (desorption) efficiency (%).

Appendix S2

The **pseudo-first-order model** is one of the first models to describe the adsorption rate. The model assumes that adsorption process is mainly controlled by diffusion, and adsorption rate is proportional to the equilibrium absorption capacity at time *t*. Its expression is:

$$Q_t = Q_e(1 - e^{-k_1 t}) \quad , \qquad \text{(S7)}$$

where k_1 (min^{-1}) is the rate constant of pseudo-first-order adsorption;Q_e (mg/g) and Q_t (mg/g) is the adsorption capacity of adsorbent at equilibrium and time *t*, respectively. *t* (min) is the contact time.

The **pseudo-second-order model** assumes that adsorption rate is mainly controlled by chemical adsorption mechanism. The nonlinear equations is as follow:

$$Q_t = \frac{k_2 Q_e^{\,2} t}{1 + k_2 Q_e t} \quad , \qquad \text{(S8)}$$

where k_2 (g/mg/min) is the rate constant of pseudo-second-order adsorption; $k_2 Q_e^{\,2}$ (mg/g/min) is defined as initial adsorption rate of adsorbent, which is proportional to the square of the equilibrium adsorption capacity.

Elovich model is an empirical formula, describing a process which contains a series of reaction mechanisms, such as the spread of the solute in the liquid phase or interface, the activation and inactivation effect. The formula is as follow:

$$Q_t = \frac{1}{\beta}\ln(\alpha\beta) + \frac{1}{\beta}\ln t \quad \text{simplified as:} \quad Q_t = A + B\ln t \quad , \qquad \text{(S9)}$$

where: α (mg/g/min) is the initial adsorption rate; β (g/mg) is a constant which is related to surface coverage and activation energy; Q_t (mg/g) is the adsorption capacity at time *t*; *t* (min) is the contact time.

Appendix S3

Langmuir monolayer adsorption theory are based on four hypotheses: 1) uniform surface; 2) monolayer adsorption; 3) each adsorption site only accommodates an adsorbate molecule; 4) no interaction among adsorbate molecules.

The nonlinear form of Langmuir equation is:

$$Q_e \equiv \frac{Q_m k_L c_e}{1 + k_L c_e} \quad , \qquad \text{(S10)}$$

where Q_m (mg/g) is the saturated adsorption capacity; k_L (L/mg) is association constant, reflecting the adsorption capacity, the higher the k_L,the better the adsorptioncapacity.

Freundlich adsorption isotherms a widely used empirical formula, describing the inhomogeneity on the surface of the adsorbent. The nonlinear form of Freundlich equation is:

$$Q_e = k_F c_e^{1/n} \quad , \qquad \text{(S11)}$$

where c_e (mg/L) is the concentration of the adsorbate when adsorption equilibrium; k_F ((mg/g)/(mg/L)$^{1/n}$) is the adsorption equilibrium constant; $1/n$ is the constant associated with adsorption affinity.

Temkin equation describes the energy relationship that adsorption heat reduced linearly with the adsorption capacity, belonging to chemical adsorption. The equation is expressed as:

$$Q_e = \frac{RT}{b} \ln A + \frac{RT}{b} \ln C_e \quad , \qquad \text{(S12)}$$

where b (kJ/mol) is the adsorption heat in Temkin isotherm; A (L/g) is the equilibrium bond constant, which is related to the maximum bond energy; R is the universal gas constant, 8.314×10^{-3} J/(mol·K).

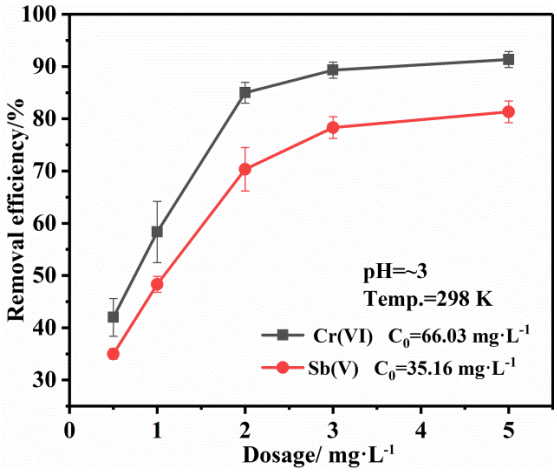

Fig. S1 The adsorption efficiency for Cr(VI) and Sb(V) at different dosages of PANI/TiO_2

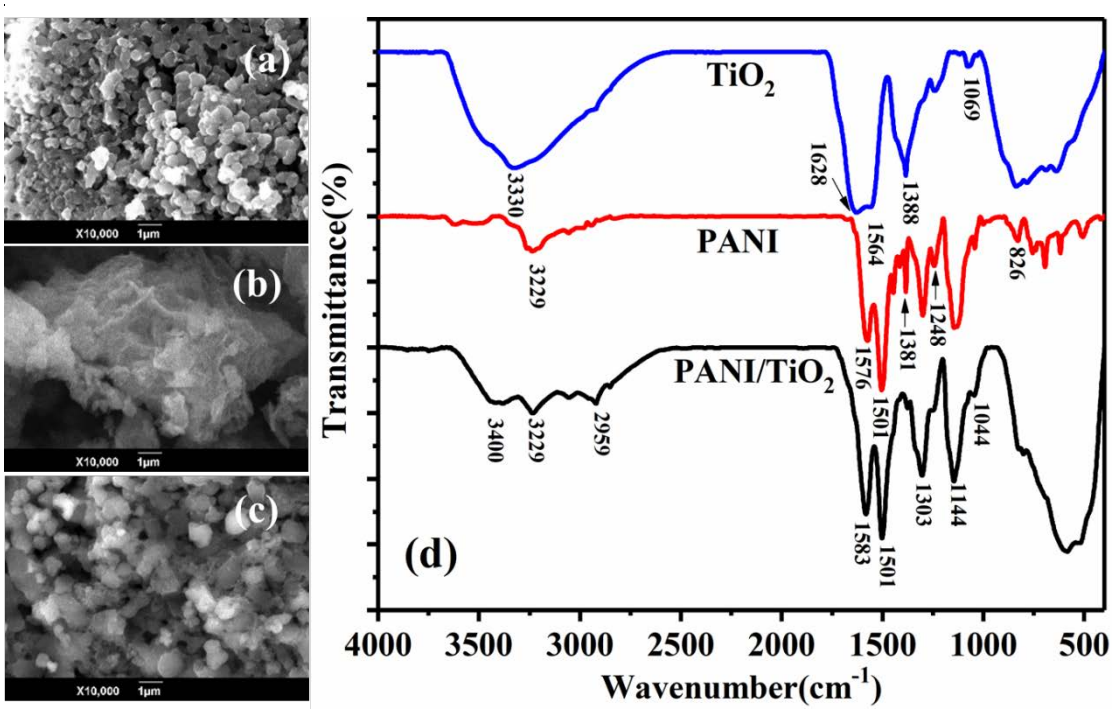

Fig. S2 The SEM images of the PANI/TiO_2 (a), PANI (b) and TiO_2 (c) and the FTIR (d)

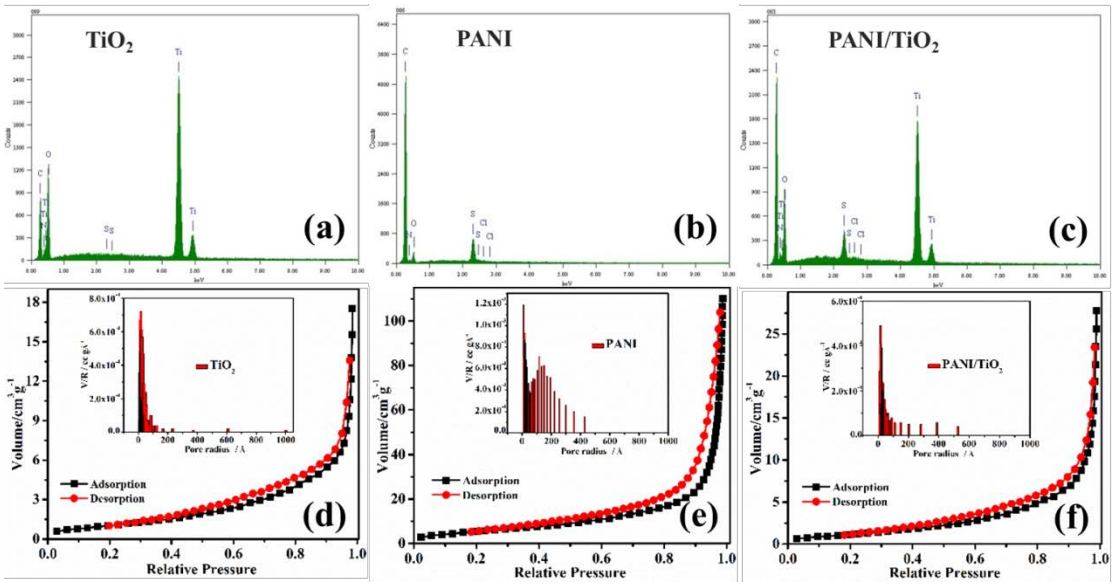

Fig. S3 EDS (a, b, c) and N_2 adsorption-desorption curves (d, e, f) of TiO_2, PANI and PANI/TiO_2

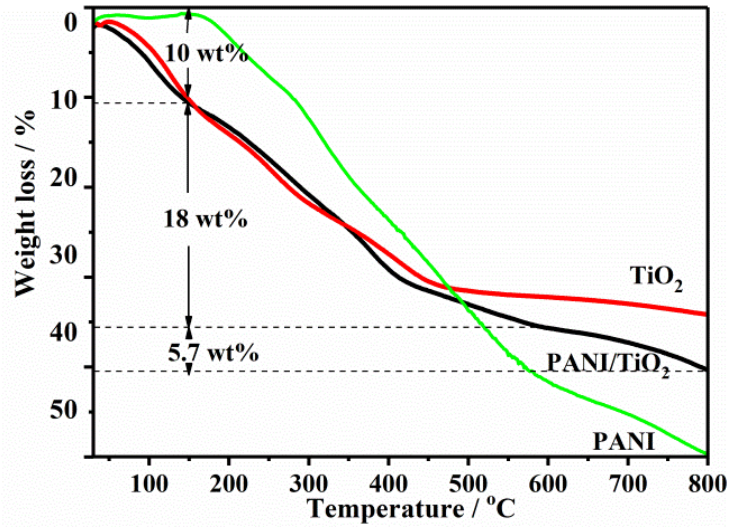

Fig. S4 The thermal stability of of TiO_2, PANI and PANI/TiO_2

As can be seen from the Fig. S4, the mass of PANI began to lose rapidly from 180℃, and the curve declined gently from 600℃ to 800℃. The weight loss percentage of the whole process was 55wt%, including hydroxyl decomposition, carboxyl decomposition, amino chain dissociation, and phenyl ring-opening decomposition. The thermal stability of TiO_2 and PANI/TiO_2 were similar, showing a three-stage thermogravimetric process.

1) The first stage of thermal weight loss occured before 150℃, which was considered to be the desorption process of bound water and adsorbed anions in the synthesis process.

2) 150℃–580℃ was the main stage of thermal decomposition, and the weight loss percentage in this stage was 18wt%. The weight loss was mainly caused by condensation of hydroxyl groups in TiO_2 and decomposition of PANI chain. When the temperature was higher than 300℃, the decrease of thermal stability of PANI/TiO_2 was significantly greater than that of TiO_2, indicating that the weight loss after this temperature was mainly due to the decomposition of PANI.

3) The last weight loss process of PANI/TiO_2 was over 580℃, with a weight loss percentage of 5.7wt %, indicating further decomposition of PANI. The thermal weight loss of TiO_2 at this stage was not obvious, and it was mainly a thermal phase transition process.

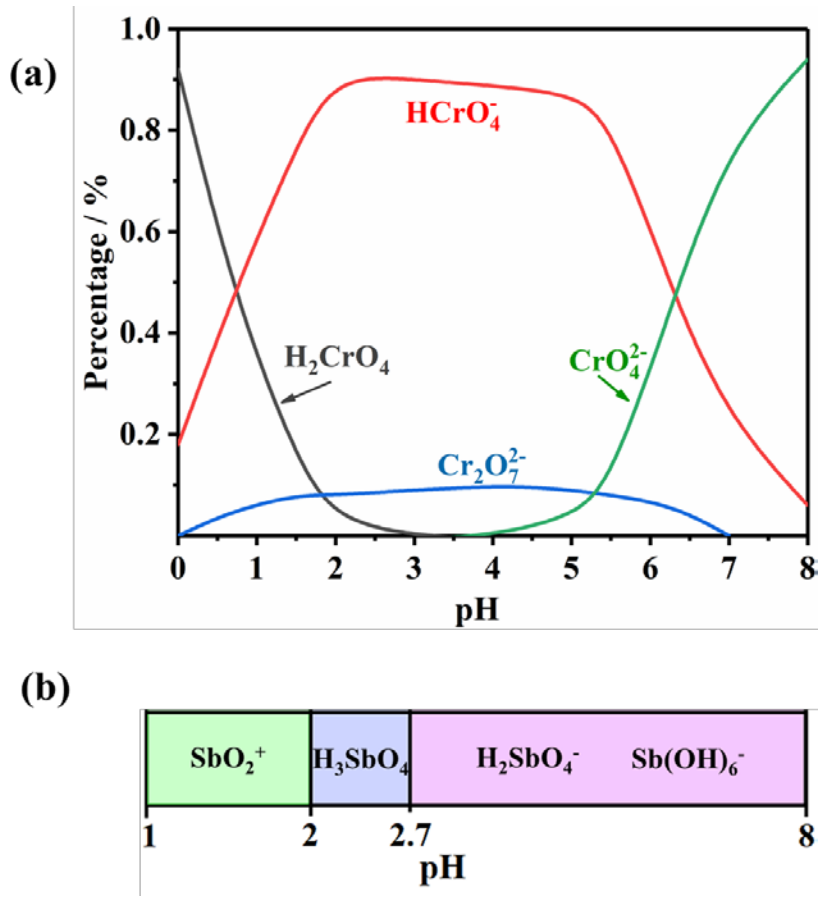

Fig. S5 The distributions of Cr(VI) and Sb(V) species as functions of solution pH: (a) Cr(VI); (b) Sb(V)

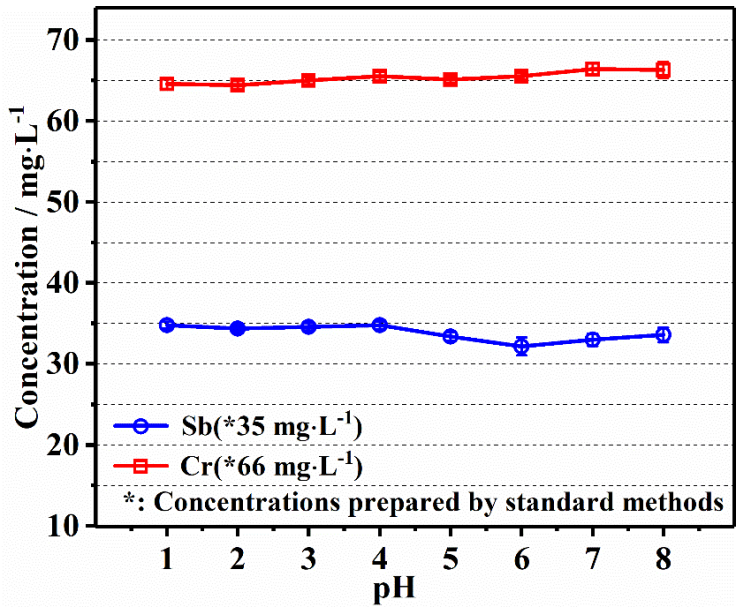

Fig. S6 The change of chromium ion and antimony ion concentration with pH

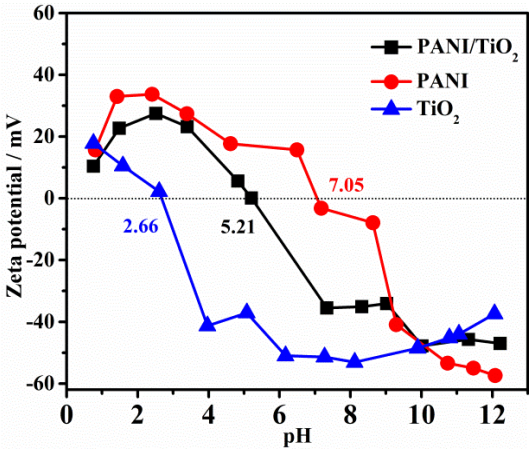

Fig. S7 ZETA potentials of TiO_2, PANI and PANI/TiO_2 (5 mg dissolved into 10^{-3} mol/L NaCl solution; HCl and NaOH for pH adjustment)

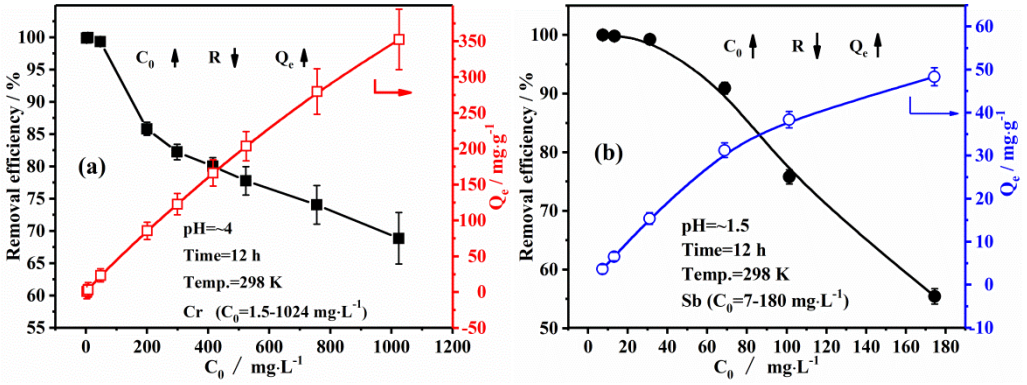

Fig. S8 Effect of initial concentration of heavy metal ions on the adsorption removal rate and equilibrium adsorption capacity: (a) Cr(VI); (b) Sb(V)

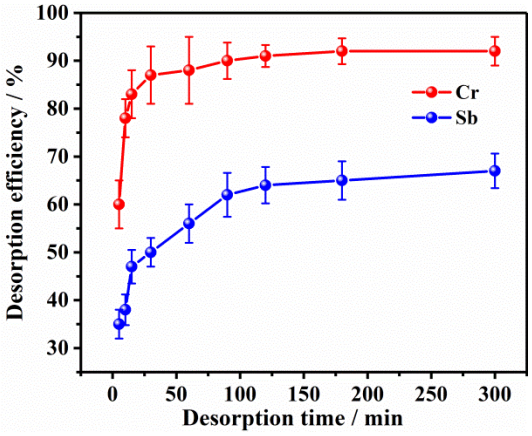

Fig. S9 Change of desorption efficiency with time

(desorption pH at 7–8, desorption agent: 0.1 mol/L NaOH, 298K)

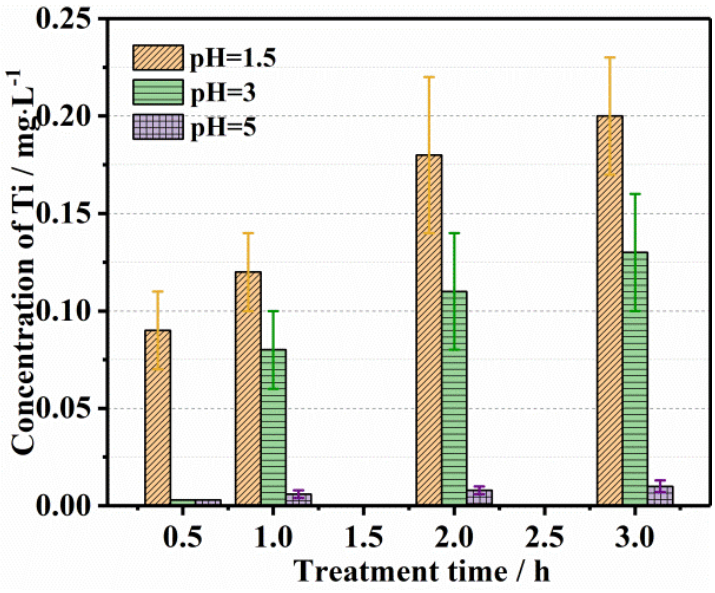

Fig. S10 Dissolution concentration of Ti after soaking PANI/TiO_2 at different pH and time

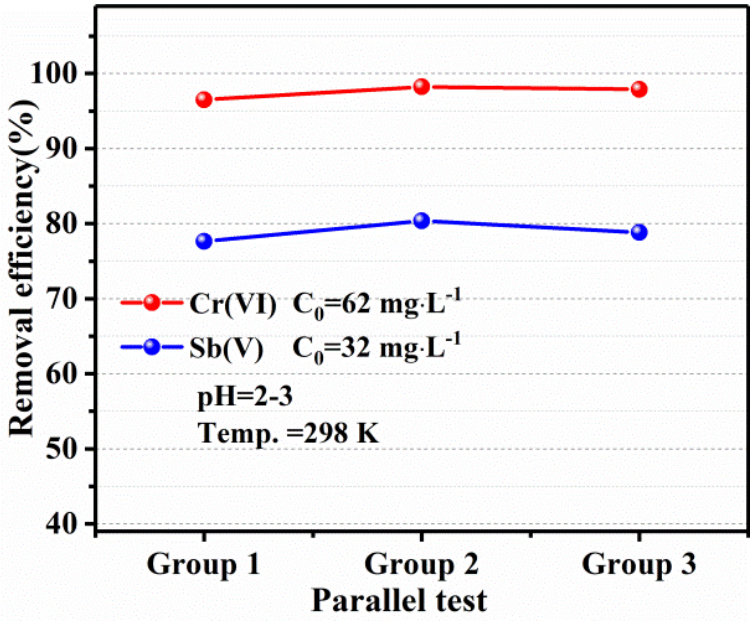

Fig. S11 The co-adsorption of Cr(VI) and Sb(V)

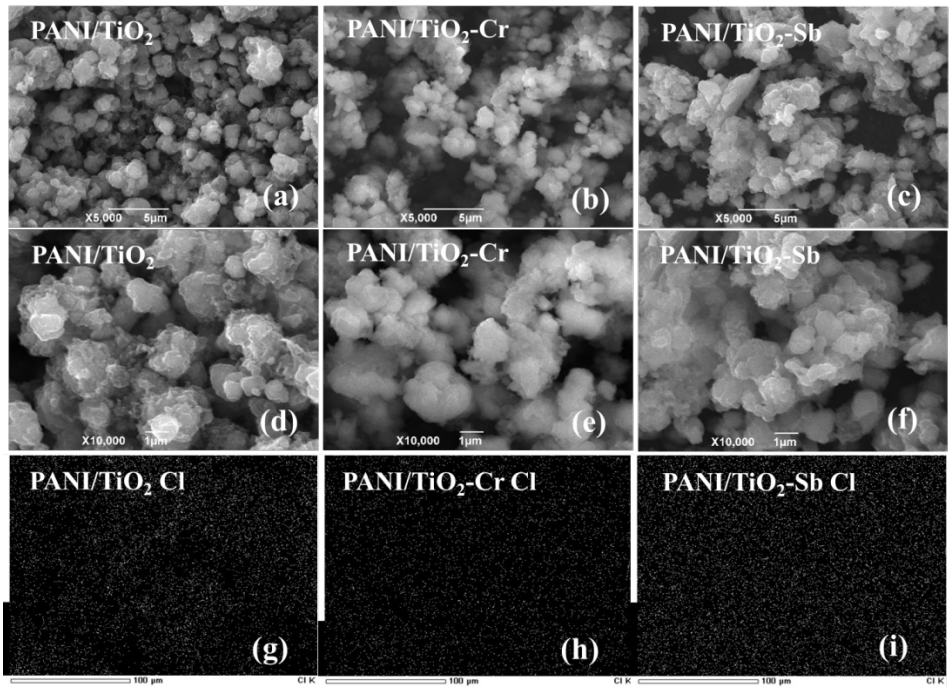

Fig. S12 SEM and EDS-Mapping (Cl) of adsorbent before and after adsorption: (a) and (d) SEM of PANI/TiO_2 before adsorption; (b) and (e) SEM of PANI/TiO_2 after Cr(VI) adsorption; (c) and (f) SEM of PANI/TiO_2 after Sb(V) adsorption; (g) EDS-Mapping (Cl) of PANI/TiO_2 before adsorption; (h) EDS-Mapping (Cl) of PANI/TiO_2 after Cr(VI) adsorption; (i) EDS-Mapping (Cl) of PANI/TiO_2 after Sb(V) adsorption

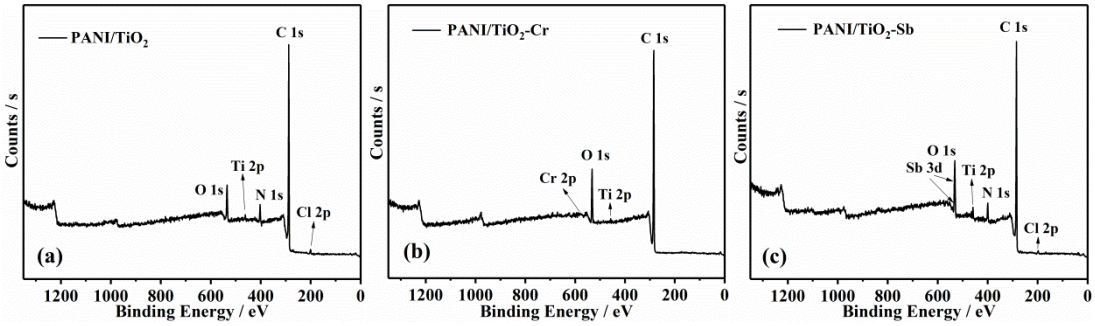

Fig. S13 XPS characterization of composite adsorbent before and after Cr(VI) and Sb(V) adsorption: (a) PANI/TiO_2; (b) PANI/TiO_2-Cr(VI); (c) PANI/TiO_2- Sb(V)

Table S1 The surface properties of the samples

Samples	S_{BET} (m^2/g)	V (cm^3/g)	R (nm)
PANI/TiO_2	11.894	0.0838	14.09
TiO_2	5.235	0.0290	11.09
PANI	19.214	0.1175	12.23
PANI/TiO_2+Cr	9.235	0.0352	11.76
PANI/TiO_2+Sb	8.943	0.0672	10.31

As can be seen from the table, the pore radius of PANI/TiO_2 is 14.09 nm, which is much larger than the hydration radius of co-existing ions. Therefore, BET data had little influence on the adsorption selectivity. The specific surface area (S_{BET}) and void radius (R) of PANI/TiO_2 after Cr(VI) or Sb(V) adsorption decreased significantly, which may be related to the adsorption and deposition of heavy metal ions, and erosion may also exist in the adsorption process.

Table S2 Adsorption kinetics parameters of Cr(VI) and Sb(V) onto composite adsorbent by Pseudo-first-order model

Metal ions	T/K	k_1 (min^{-1})	Q_e (mg/g)	Q_e (exp.)	R^2	S.D.
Cr(VI)	298	0.4017	33.48	34.55	0.9924	0.75
	308	0.5449	35.55	36.90	0.9934	0.76
	318	0.4791	35.51	36.73	0.9916	0.83
Sb(V)	298	0.0199	25.35	29.03	0.8713	3.07
	308	0.0221	34.98	38.86	0.9283	2.91
	318	0.0289	31.18	35.35	0.8516	3.65

Table S3 Adsorption kinetics parameters of Cr(VI) and Sb(V) onto composite adsorbent by Pseudo-second-order model

Metal ions	T/K	k_2 (g/mg/min)	Q_e (mg/g)	Q_e (exp)	$k_2Q_e^2$ (mg/g/min)	R^2	S.D.
Cr(VI)	298	0.0185	34.48	34.55	22.03	0.9999	1.07
	308	0.0168	36.76	36.90	22.78	0.9999	1.76
	318	0.0154	36.76	36.73	20.79	0.9999	1.69
Sb(V)	298	9.44E−4	29.58	29.03	0.8266	0.9897	2.11
	308	7.72E−4	40.32	38.86	1.2547	0.9944	2.12
	318	9.94E−4	36.50	35.35	1.3234	0.9946	2.59

Table S4 Adsorption kinetics parameters of Cr(VI) and Sb(V) onto composite adsorbent by Simple Elovich equation

Metal ions	T (K)	A (a.u.)	B (mg/g)	R^2	S.D.*
Cr(VI)	298	29.11	0.9434	0.8873	0.99
	308	32.45	0.7092	0.9752	0.15
	318	31.61	0.8264	0.9557	0.26
Sb(V)	298	–1.90	4.7619	0.9797	0.91
	308	–3.67	6.6667	0.9715	1.51
	318	0.48	5.5555	0.9831	0.97

Notes: *, The validity of the models used in manuscript was determined by standard deviation (S.D.) by the following equation:

$$S.D. = \sqrt{\frac{1}{N}\sum_{i=1}^{N}\left(q_{\exp} - q_{cal}\right)^2}, \quad \text{(S13)}$$

where: q_{exp} and q_{cal} are the experimental data and theoretical calculating values of q_t or q_e.

Table S5 EDS analysis data before and after Cr(VI) and Sb(V) adsorption *

Samples	C	O	Cl	Ti	Cr	Sb	Na
Ad+NaOH	57.86	28.64	0.04	12.04	–	–	1.26
Ad+NaOH+HCl	46.22	25.8	1.49	26.25	–	–	0.03
Ad+NaOH+HCl+Cr	54.33	30.03	0.12	13.05	2.34	–	0.02
Ad+NaOH+HCl+Sb	50.96	27.49	1.20	18.87	–	1.15	0.09

Notes: *, wt %; Ad, PANI/TiO_2

Table S6 Assignments for FTIR adsorption bands

Wavenumber (cm^{-1})				Assignment
a	b	c	d	
3407	3438	–	3430	O-H vibration
3228	3228	3236	3232	N-H vibration
3045	3045	3062	3045	C-H vibration in benzene ring
1586	1582	1586	1586	C=C stretching vibration in quinone ring
1503	1498	1507	1503	C=C stretching vibration in benzene ring
1381	1381	1386	1381	C-N /N-O stretching vibration in QBQ
1302	1302	1307	1302	C-N vibration in N-B-N
1237	1241	1246	1237	C-N stretching vibration in BBB
1168	–	1172	1172	N=Q=N vibration
–	1150	–	1145	$Q=N^+H$-B vibration
–	881	–	–	Up-and-down vibration of the aromatic ring skeleton
827	823	827	823	C-H out-of-plane bending of 1,4-ring
–	800	–	800	C-H out-of-plane bending of 1,2-ring
500–700	500–700	500–700	500–700	Ti-O-Ti bending mode

Table S7 Adsorption efficiencies of Cr(VI) (C_0=50 mg/L) and Sb(V) (C_0=37 mg/L) by PANI, TiO_2 and PANI/TiO_2

Metal ions	PANI/TiO_2	TiO_2	PANI
Cr(VI)	98.65%	58.51%	72.48%
Sb(V)	97.48%	71.78%	12.81%

Table S8 XPS peak position after Cr(VI) and Sb(V) adsorption by PANI/TiO_2

Elements	PANI/TiO_2	PANI/TiO_2-Cr	PANI/TiO_2-Sb	Assignments
C 1s	284.6	284.4	284.4	C-C/C-H
	285.8	285.6	285.8	C-N
O 1s	530.8	531.4	527.2	lattice oxygen O_{latt}
	532.0	532.2	529.0	Adsorbed oxygen O_{ad}
	533.2	533.3	530.1	H_2O
N 1s	398.9	398.6	–	=N-
	399.6	399.4	396.3	-NH-
	400.9	400.4	397.5	$-NH^+-/=N^+-$
Ti 2p	458.9	458.7	456.0	2p 3/2
	–	–	461.7	2p 1/2